Competing local orders in liquid and amorphous structures of Ge2Sb2Te5: Influence of exchange-correlation functional

Kye Yeop Kim, Deok-Yong Cho, Byung-ki Cheong, Dohyung Kim, Hideki Horii et al.

Competing local orders in liquid and amorphous structures of Ge$_2$Sb$_2$Te$_5$: Influence of exchange-correlation functional

Kye Yeop Kim,[1] Deok-Yong Cho,[2] Byung-ki Cheong,[3] Dohyung Kim,[4] Hideki Horii,[4] and Seungwu Han[1,a)]

[1]*Department of Materials Science and Engineering, Research Institute of Advanced Materials (RIAM), Seoul National University, Seoul 143-747, South Korea*
[2]*IWE2 & JARA-FIT, RWTH Aachen University, 52056 Aachen, Germany*
[3]*Electronic Materials Center, Korea Institute of Science and Technology, Seoul 136-791, South Korea*
[4]*Process Development Team, Semiconductor R&D Center, Samsung Electronics, Co., Ltd., Hwasung 445-701, South Korea*

Liquid and amorphous structures of Ge$_2$Sb$_2$Te$_5$ are theoretically studied with various exchange-correlation functionals. It is found that the balance of competing local orders around Ge atoms is substantially affected by the functional type, and the hybrid functional leads to structures that are in best agreement with experiment. The delocalization error inherent in semilocal functionals results in over-population of octahedral Ge configurations, which is compounded by the limitation of melt-quench processes in identifying the most stable amorphous structure. The present work underscores the importance of functional choice when competing local orders present in disordered systems. © *2013 American Institute of Physics.* [http://dx.doi.org/10.1063/1.4798380]

I. INTRODUCTION

Modeling disordered systems such as liquid and amorphous phases constitute one of the biggest challenge in modern computational materials science due to several technical hurdles. For one thing, the absence of structural periodicity necessitates the computationally expensive supercell approach. In addition, due to the dearth of experimental information on short- or medium-range orders, atomic structures should be obtained without any experimental guidance. While in liquid, the equilibrium can be established within a relatively short simulation time owing to fast atomic diffusion, intrinsic slow relaxation in the amorphous phase causes the melt-quench process, the widely-used computational approach, to often result in structures that are at variance with a global minimum. The best-known examples are over-coordination in *a*-Si[1] and wrong bonds in *a*-GaAs.[2]

Recently, the discrepancy between theoretical and experimental amorphous structures of Ge$_2$Sb$_2$Te$_5$ (GST), a key material in the phase-change memory,[3] rekindle the above long-standing issue. It is widely accepted that the contrasting electrical and optical properties between crystalline and amorphous GST (*c*-GST and *a*-GST, respectively) are results of a dramatic change in local order, particularly around Ge atoms.[4] This was first revealed by the extended X-ray absorption fine structure (EXAFS) experiment that showed a significant reduction of the Ge-Te bond length by 0.22 Å upon amorphization.[5] This finding was ensued by a series of first-principles simulations to obtain *a*-GST in a melt-quench style, resulting in overall reasonable agreements with experiment.[6–10] However, the reduction of the Ge-Te bond length is significantly underestimated in all theoretical works

and only about 0.1 Å shortening was obtained. This is mainly because the Ge-Te bonds in *a*-GST are substantially longer than measured values. It is noted that this is not related to the well-known overestimation of bond lengths in generalized gradient approximation; the local density approximation also shows a similar disagreement. Considering typical accuracy of density functional calculations on structural properties, this overestimation should be considered seriously.

The structural disparity between theory and experiment is in fact related to competing local orders in *a*-GST. In theoretically melt-quenched *a*-GST, it was found that octahedral and tetrahedral Ge (*o*-Ge and *t*-Ge, respectively) atoms coexist.[6] Being close to the structural unit in crystal, *o*-Ge atoms tend to maintain longer Ge-Te bonds. If *t*-Ge atoms are considered separately, the Ge-Te bond length is close to the experimental value.[11] This is further supported by an *a*-GST structure that contains only *t*-Ge atoms.[12] Therefore, it is inferred that *a*-GST in experiment is abundant with *t*-Ge atoms, while theoretically melt-quenched *a*-GST is dominated by *o*-Ge atoms. The liquid phase of GST (*l*-GST) also shows similar disagreements, i.e., the Ge-Te bond length in the simulation[13] is longer than EXAFS data[14] by ∼0.2 Å, suggesting that structural motifs are quite different between theory and experiment as in the amorphous phase.

The significant discrepancy between theory and experiment in the foregoing discussion puts two computational ingredients under scrutiny. Firstly, for *a*-GST, the melt-quench process may not yield the most stable structure among possible metastable states as mentioned above. Secondly, it can be questioned whether the exchange-correlation functional of Perdew-Becke-Ernzerhof (PBE),[15] which is used predominantly in the first-principles studies on GST, is the right choice for the present system. For instance, it was reported that simulated structures of *l*-GeSe$_2$ improved

a)Electronic mail: hansw@snu.ac.kr

substantially when a correlation functional is used that is not based on the uniform electron gas.[16] In this article, we try to address these issues by employing various exchange-correlation functionals, notably including hybrid functionals.

II. COMPUTATIONAL METHODS

We use the Vienna *ab initio* simulation package (VASP) for the first-principles MD simulations and electronic structure calculations.[17] The electron-ion interaction is described by projected-augmented-wave (PAW) pseudopotential.[18] For exchange-correlation functionals of the semilocal type, we employ PBE and Becke-Lee-Yang-Parr (BLYP),[19,20] with distinct natures in the correlation energy. We also consider the hybrid functional proposed by Heyd-Scuseria-Ernzerhof (HSE06).[21] As the fraction of the exact exchange energy, 0.25 and 0.5 are used (denoted as HSE-*q* and HSE-*h*, respectively). While the quarter fraction is theoretically supported by the perturbation theory[22] and gives reasonable band gaps for most oxides[23] and hence would be a sound choice in GST as well, the results with HSE-*h* are useful in understanding the influence of the exact exchange term more clearly. We note that the fraction of exact exchange tends to decrease with the dielectric constant.[24] According to this relation, the fraction could be smaller than 0.25 in *a*-GST.

Since the computation with hybrid functionals is very costly, a relatively small supercell comprising 72 atoms is used throughout this work. However, a systematic comparison within PBE and BLYP using larger supercells showed that size effects on the local order is not significant in liquid and amorphous structures. In simulating liquid structures, the energy cutoff of 250 eV and single *k*-point of (1/4,1/4,1/4) are used. The mesh grids for the fast-Fourier transform and the Fock potential are chosen to ensure the convergence of energy, stress, and atomic forces within 10 meV/atom, 10 kbar, and 0.05 eV/Å for a given liquid snapshot. For melt-quench simulations, we lower the computational accuracy to 130 eV for the energy cutoff and Γ-point sampling. Even though this parameter set results in some errors in individual atomic forces, the average dynamics is similar to the reference data as can be inferred from the comparison of radial distributions. The final relaxation of the melt-quenched *a*-GST is carried out with the parameter set used in the liquid simulation, and lattice vectors as well as atomic positions are fully relaxed.

In obtaining the radial distribution function [RDF; $g(r)$] from the partial RDF [$g_{\alpha\beta}(r)$], we consider different scattering factor of each atom for comparison with experimental data:

$$g(r) = \frac{\sum_{\alpha,\beta} c_\alpha c_\beta f_\alpha f_\beta g_{\alpha\beta}(r)}{\left(\sum_\alpha c_\alpha f_\alpha\right)^2}, \qquad (1)$$

where c_α and f_α indicate atomic fraction and scattering factor of element α, respectively. In the case of X-ray diffraction, we assume that the atomic form factor is not sensitive to spatial frequency and replace f_α with atomic number (Ge: 32, Sb: 51, Te: 52). For the neutron diffraction, the scattering

factor can be replaced with scattering lengths that are 8.185, 5.57, and 5.80 fm for Ge, Sb, and Te, respectively.[27]

III. RESULTS AND DISCUSSIONS

A. Liquid structure

We first examine liquid structures. The starting configuration was prepared by randomly distributing 8 formula units of GST into a cubic box with a length of 13.4 Å which corresponds to the experimental liquid density of 0.030 atoms · Å^{-3} at 1073 K.[28] The structure was pre-melted at 2000 K for 12 ps and then equilibrated at 900 K for 30 ps. The structural information was collected during the last 15 ps.

The RDFs for *l*-GST are presented in Fig. 1(a). As a reference, the Fourier-transformed X-ray diffraction data from Ref. 25 is also shown. It is seen that the first-peak position in the PBE result is longer than the experimental value (the vertical dashed line) by 0.15 Å. In addition, the medium-range order at ~4 Å is rather broad. On the other hand, with BLYP and HSE, the first peaks shift to smaller values and the medium-range order becomes more featured. Overall, it can be concluded that RDFs computed with BLYP or HSE-*q* are most consistent with experiment. The narrow distribution in the medium-range order for HSE-*h* originates from Te-Te correlations as will be explained below.

Table I enlists Ge-Te and Sb-Te bond lengths read from the first-peak position of the corresponding pair distribution function. The EXAFS data at 900 K are also provided.[14] To be consistent with the analysis on RDF, the bond lengths are significantly overestimated in PBE. With BLYP or HSE functionals, improvements are noticeable and HSE-*h* results are in best agreement with experiment on the local bond lengths.

To understand structural variations with functional types, we analyze order parameters around each atom. The following formula is adopted to define the order parameter α_i for the *i*th atom:[13]

$$\alpha_i = \frac{1}{6}\sum_{j\neq i} f(r_{ij}) \frac{\sum_{k\neq i,j} f(r_{ik}) g(\theta_{ijk})}{\sum_{k\neq i,j} f(r_{ik})}, \qquad (2)$$

where $f(r_{ij}) = 1/(\exp[\kappa^{-1}(r_{ij}-r_0)]+1)$ is a weight factor depending on the bond length, with the broadening parameter (κ) of 0.05 Å and cutoff length (r_0) of 3.2 Å. In Eq. (2),
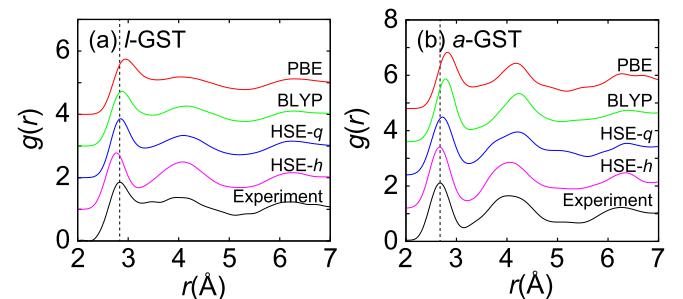

FIG. 1. The radial distribution functions [$g(r)$] of (a) *l*-GST and (b) *a*-GST computed with various exchange-correlation functionals. The experimental diffraction data for *l*-GST at 953 K (Ref. 25) and *a*-GST[26] are shown as dashed lines. The vertical dashed lines indicate the first peak positions in experimental RDFs.

TABLE I. The Ge-Te and Sb-Te bond lengths in liquid and amorphous GST. For comparison, the averaged short bonds in the rocksalt phase of GST (*c*-GST) are also shown.

		PBE	BLYP	HSE-*q*	HSE-*h*	Exp.
l-GST	Ge-Te	2.83	2.76	2.76	2.65	2.64[a]
(Å)	Sb-Te	2.98	2.93	2.89	2.83	2.85[a]
a-GST	Ge-Te	2.78	2.74	2.67	2.62	2.60−2.63[b]
(Å)	Sb-Te	2.93	2.86	2.86	2.79	2.82−2.85[b]
c-GST	Ge-Te	2.90	2.85	2.84	2.81	2.81−2.85[c]
(Å)	Sb-Te	3.01	2.97	2.95	2.92	2.87−2.92[c]

[a]Reference 14.
[b]References 5, 36, and 37.
[c]References 5 and 38.

$g(\theta_{ijk}) = \cos^2[2(\theta_{ijk} - \pi/2)]$ is an angular weight function for the angle θ_{ijk}. The coordination number, CN, of the *i*th atom is calculated as $\sum_{j \neq i} f(r_{ij})$.

Figure 2 shows population maps of Ge, Sb, and Te atoms with certain order parameters and CNs, averaged over 15 ps during simulations. The slant line indicates the octahedral ordering and the (4.0, 0.4) point corresponds to the ideal tetrahedral ordering. Compared to PBE results, the intensity around the tetrahedral order of Ge atoms significantly increases in HSE-*q* or HSE-*h* results. (Note that the color code in Fig. 2 is logarithmic.) The distribution with BLYP is similar to the HSE-*q* result. Therefore, the reduction of

Ge-Te bond lengths in BLYP and HSE calculations is mainly attributed to a substantial increase of the tetrahedral order in Ge atoms. For Sb and Te atoms in Figs. 2(b) and 2(c), respectively, the change in the order parameter is less pronounced in comparison with Ge atoms. Nevertheless, it can be seen that the distribution of the order parameter becomes sharper and the number of two-fold Te atoms increases with the hybrid functional. Since Sb or Ge atoms in HSE-*h* calculations favor well-defined local orders with small fluctuations, Te-Te pairs surrounding them exhibit a narrow length distribution at ∼4 Å as shown in Fig. 1(a).

By monitoring temporal evolution of the order parameter, we also find that Ge atoms in PBE simulations rapidly fluctuate between *o*-Ge and *t*-Ge configurations, implying a smooth energy landscape. This is consistent with a broad distribution of order parameters in Fig. 2(a).

B. Amorphous structure

Next, we discuss on *a*-GST generated through melt-quench processes. The pre-melting at 2000 K is carried out for 12 ps using PBE, followed by 30-ps liquid simulation at 900 K according to each functional. The liquid structure is then cooled down to 300 K with the cooling rate of −15 K/ps. The structure is finally relaxed fully at 0 K. As mentioned above, due to the sheer computational cost, we have employed different sets of computational parameters during melt-quench and relaxation stages.
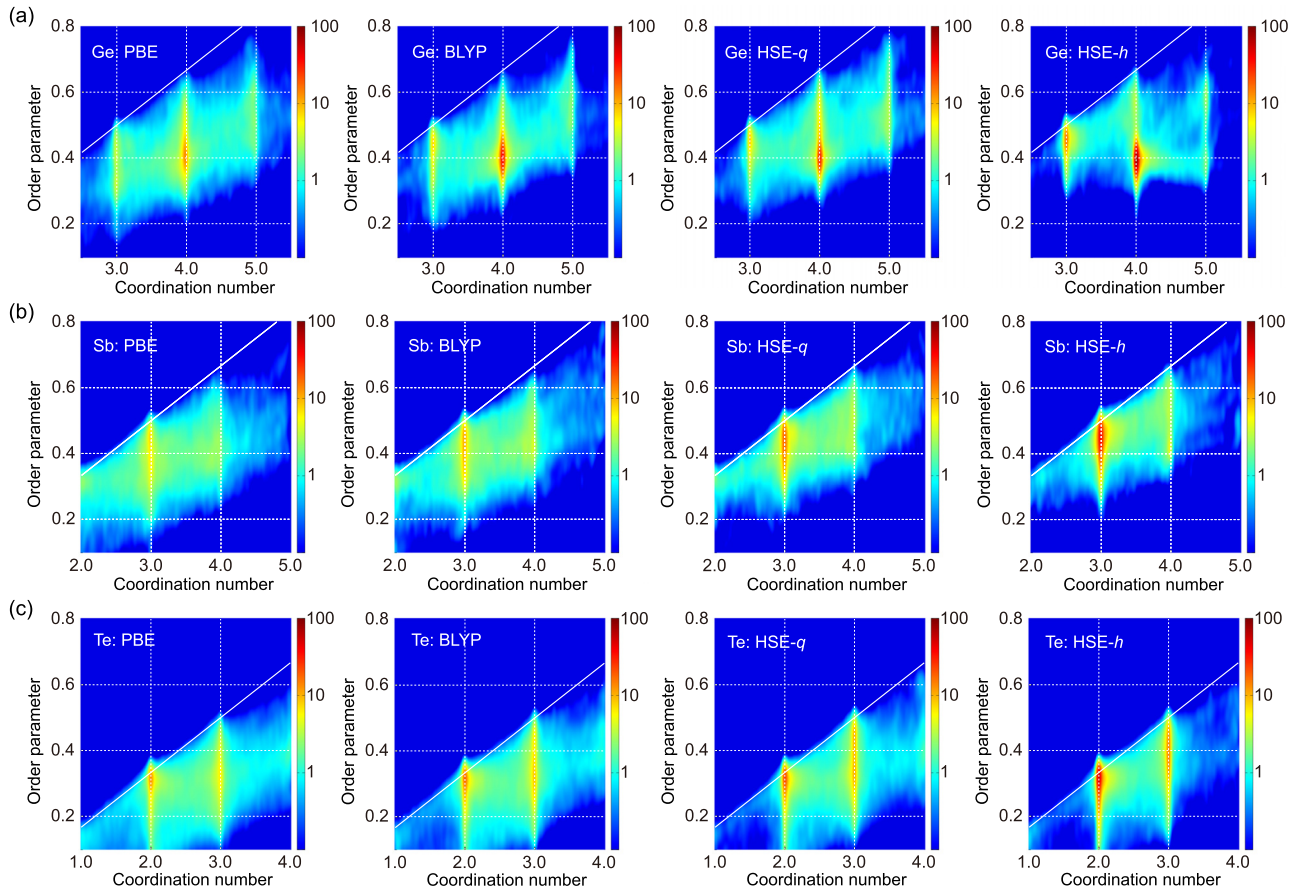

FIG. 2. Population maps of (a) Ge, (b) Sb, and (c) Te atoms in *l*-GST with respect to the order parameter and coordination number. The slant line indicates the octahedral ordering while the tetrahedral order is represented by the (4.0, 0.4) point.
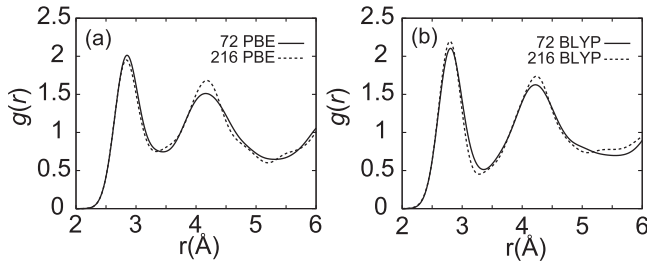
FIG. 3. Radial distribution functions of *a*-GST for 72 - and 216-atom super-cells computed with (a) PBE and (b) BLYP functionals.

Figure 1(b) shows RDFs of simulated *a*-GST in comparison with the Fourier-transformed neutron diffraction data of as-deposited GST.[26] Several observations are in common with *l*-GST; for PBE, the first-peak position is shifted outward and the medium-range order at 3 ~4 Å is much smoother than experiment. The agreement is improved in other functionals and the best match is achieved by HSE-*q* or HSE-*h*. Consistently, Ge-Te and Sb-Te bond lengths measured by EXAFS are well reproduced by HSE functionals (see Table I).

In order to check the influence of the supercell size, we carry out melt-quench simulations with 216 atoms for PBE and BLYP functionals. Figure 3 compares the total RDFs of *a*-GST between 72 - and 216-atom supercells. It is seen that RDFs agree well, particularly within the first shell, indicating that the 72-atom cell is enough for examining the short-range orders.

For more direct comparison with experiment, we simulate EXAFS signals using the FEFF8 code.[29] In detail, a muffin-tin potential with automatic overlapping is used for the approximate potential in the ground state, while for the effective one-particle scattering potential in the excited states, Hedin-Lundqvist exchange correlation is employed. The contribution of thermal disorder is also considered using a correlated Debye model[30] with a Debye temperature of 300 K.[31] This effectively reduces the magnitude of the

TABLE II. Structural properties and relative energies of *a*-GST; the peak position in the angular distribution function (ADF), portion of *t*-Ge among fourfold Ge atoms, coordination numbers (CNs) around each atom (cutoff radius of 3.2 Å) and energy difference between amorphous and crystalline GST.

| | ADF peak (°) | *t*-Ge (%) | Coordination number | | | ΔE_{a-c} (meV/atom) |
			Ge	Sb	Te	
PBE	92	33	3.7	3.2	2.6	106
BLYP	98	42	3.4	3.0	2.4	74
HSE-*q*	104	59	3.7	3.2	2.4	98
HSE-*h*	106	60	3.7	3.1	2.2	50
Exp.	…	…	3.8-3.9[a]	2.8-3.1[a]	2.0-2.4[a]	44[b]

[a]References 5, 36, and 37.
[b]Reference 39.

EXAFS oscillation at high *k* values. The *k* scale is obtained by shifting the theoretical energy scale by 0.8 Ry to align the vacuum level.[11] The results are shown in Fig. 4. The experimental EXAFS data for the as-deposited sample[26] are presented as a reference. It is clearly seen that EXAFS oscillations simulated with the HSE models are in much better agreement with experiment than PBE data. The comparison with the EXAFS signal for the laser-amorphized sample[5] is also compared (not shown here) and again, HSE models are superior to the PBE model. We note that the simulated EXAFS signal from the as-deposition simulation in Ref. 11 is similar to HSE-*q* results.

The local order around Ge atoms, i.e., *o*-Ge or *t*-Ge, is first examined in Table II by the peak position in angle distribution functions (ADFs). It is observed that the peak shifts from 90° in PBE, characteristic of *o*-Ge, towards 109.5° of *t*-Ge by HSE. The population of *t*-Ge atoms in Table II is computed by integrating order parameters between 0.3 and 0.5 for four-fold coordinated Ge atoms during 2-ps annealing at 300 K. It is seen that *t*-Ge atoms are almost doubled in HSE results. In Table II, CN for each element within the cutoff radius of 3.2 Å is also presented. Atom-resolved CNs are shown in Table III. Most notably, CN for Te is significantly reduced to 2.2-2.4 when HSE functionals are used, indicating
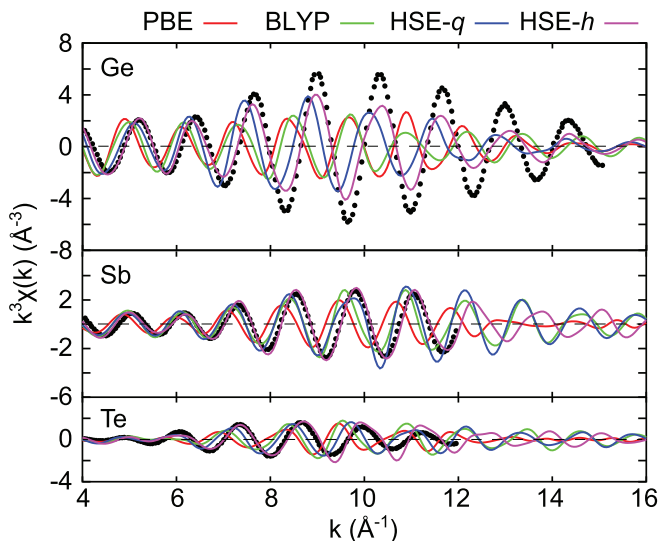

FIG. 4. Simulated EXAFS oscillations of Ge, Sb and Te *K*-edges using melt-quenched amorphous structures. Black dots are experimental results.[26]

TABLE III. Atom-resolved coordination numbers in *a*-GST obtained through melt-quench simulations with various exchange-correlation functionals.

	PBE	BLYP	HSE-*q*	HSE-*h*
Ge-Ge	0.4	0.2	0.6	0.4
Ge-Sb	0.3	0.1	0.4	0.4
Ge-Te	3.1	3.0	2.7	2.9
Ge (total)	3.7	3.4	3.7	3.7
Sb-Ge	0.3	0.1	0.4	0.4
Sb-Sb	0.6	0.4	0.3	0.5
Sb-Te	2.3	2.6	2.6	2.2
Sb (total)	3.2	3.0	3.2	3.1
Te-Ge	1.2	1.2	1.1	1.2
Te-Sb	0.9	1.0	1.0	0.9
Te-Te	0.4	0.2	0.3	0.2
Te (total)	2.6	2.4	2.4	2.2

that the metallic bonding character is weakened. The last column of Table II is the energy difference between amorphous and cubic crystalline structures, showing that the HSE-*h* result is the closest to the experimental value. The above analysis indicates unequivocally that melt-quenched *a*-GST structures generated with HSE most closely reproduce the experimental *a*-GST.

The dependence of liquid and amorphous structures on the exchange-correlation functional shows that semilocal functionals favor *o*-Ge atoms, while the *t*-Ge order tends to be stabilized by the exact exchange energy. The characteristic dependence of the local order on the functional type could be understood in terms of the electronic nature; it is well known that the uniform-gas based functionals such as PBE tends to overly delocalize electrons.[32] Such a delocalization error in PBE can affect the balance between *o*-Ge and *t*-Ge in two ways; first, it can be confirmed by the inspection of the inverse participation ratios (not shown) that states near the valence edge are more localized at higher concentrations of *t*-Ge.[33] Therefore, the delocalization tendency of PBE would favor structures abundant with *o*-Ge atoms. Second, as was pointed out in Ref. 16, the delocalization error of PBE leads to an overestimate of metallic bonding character. This would undermine the covalent nature in the tetrahedra centered around the *t*-Ge atom, and increase *o*-Ge configurations and over-coordinated Te atoms. The spurious self-interaction, which is at the heart of the delocalization error, is partly relieved by the exact exchange term in the hybrid calculation. As such, *t*-Ge atoms are more favored in hybrid functionals than in PBE.

C. Relative stability among melt-quenched structures

In the above, distinct amorphous structures resulted depending on the exchange-correlation functional. An important question here would be whether they correspond to the most stable amorphous structure for a given energy functional. This is particularly relevant in *a*-GST because two competing local orders, i.e., *o*-Ge and *t*-Ge, can lead to a complicated energy landscape. We try to address this, albeit indirectly, by switching the exchange-correlation functional for melt-quenched *a*-GST structures and relaxing them locally. For convenience, the final structure is denoted as $a(X \mapsto Y)$, where X and Y are functionals used in the melt-quench simulation and post-relaxation, respectively. The resulting energies are compiled in Table IV as a matrix form with column and row corresponding to X and Y, respectively. The energies are referenced to crystalline values and should be compared within the same row. Annealing simulations for 3 ps at 300 K confirms that the energy differences in Table IV are well maintained at ambient temperatures. In passing, it is noted that one should be mindful of the energy fluctuation between repeated simulations in interpreting the results in Table IV. From additional three runs with the PBE functional, we find that the energy fluctuation is ~5 meV/atom.

Several points are noteworthy in Table IV. First of all, surprisingly, $a(\mathrm{HSE}-h \mapsto Y)$ is the most stable for all Y's (see bold-faced numbers). Recall that this structure has the

TABLE IV. Energies of *a*-GST in meV/atom when the exchange-correlation functional is switched. Each column corresponds to the functional used in the melt-quench simulation while the functional in the post-relaxation is presented row-wise. The energies are referenced to those in cubic crystalline structures. The most stable energies are marked in bold.

Relaxation	Melt-quench simulation			
	PBE	BLYP	HSE-*q*	HSE-*h*
PBE	106	98	111	**97**
BLYP	92	74	84	**68**
HSE-*q*	100	90	98	**78**
HSE-*h*	86	72	75	**50**

largest number of *t*-Ge atoms (the post-relaxations did not affect the local order much). Therefore, the result indicates that *a*-GST enriched with *t*-Ge atoms could also be stable within PBE. However, such *a*-GST structures have not been identified in the previous melt-quench simulations as far as we are aware. This might be caused by the unrealistic quenching speed which tends to produce *a*-GST similar to *l*-GST. Furthermore, the high entropic cost[12] should disadvantage the *t*-Ge order until the temperature is well below the melting point. For the same reasons, the melt-quench simulation with HSE-*q* may have resulted in the amorphous structure that is less stable than a global minimum. Our finding is consistent with Ref. 11 in which *t*-Ge abundant structures were obtained within PBEsol from the as-deposition simulation because the entropic penalty of *t*-Ge is reduced at low-temperature conditions.

In Table IV, it is also seen that the energy difference between the most and least stable structures is widened as Y varies from PBE to HSE-*h* (from 14 to 36 meV/atom). This implies that the energy landscape of *a*-GST is "wrinkled" in PBE with several local minima stretched over a sizable range of *o*-Ge to *t*-Ge ratio. In contrast, the corresponding landscape in hybrid functionals appear to be much simpler with a distinctively low energy for the structure enriched with *t*-Ge atoms.

It has been discussed in theory[11] and experiment[34] that the as-deposited and melt-quenched *a*-GST may have different amorphous structures. Clearly, the simulated *a*-GST obtained through the melt-quench process should be more consistent with melt-quenched samples. The electron diffraction experiment in Ref. 35 showed that RDFs are similar among as-deposited, annealed, and melt-quenched samples except for a small shoulder peak at ~3.2 Å, which justifies our comparison with the as-deposited sample in Fig. 1(b). The EXAFS signal and bond lengths in Ref. 5 were measured for the melt-quenched sample and the above comparison showed that HSE models are more consistent with the experiment than the PBE model. Finally, the analysis on the X-ray absorption near edge spectrum (XANES)[34] showed that the melt-quenched sample is a mixture of *t*-Ge and *o*-Ge and this is consistent with HSE models because they include a substantial portion of *o*-Ge (see Table III). Therefore, even if the comparison with the experimental data is limited to melt-quenched samples, the HSE functional supersedes the PBE one.

IV. SUMMARY

In summary, liquid and amorphous structures of GST were investigated by first-principles MD simulations. The significant discrepancy on local order between PBE results and experiment, stemming from the delocalization error, was mostly resolved if HSE functionals were used. The improvements by employing BLYP were also substantial. Therefore, we suggest that hybrid or BLYP functionals should be favored over uniform-gas based semilocal functionals in studying disordered chalcogenides, particularly when Ge atoms are included. In general, the present work underscores the importance of functional choice when competing local orders present in a disordered system. In this case, computations with distinct exchange-correlation functionals as in this work could provide a solution.

ACKNOWLEDGMENTS

[1]M. Ishimaru, S. Munetoh, and T. Motooka, Phys. Rev. B **56**, 15133 (1997).
[2]N. Mousseau and L. J. Lewis, Phys. Rev. Lett. **78**, 1484 (1997).
[3]M. Wuttig and N. Yamada, Nature Mater. **6**, 824 (2007).
[4]B. Huang and J. Robertson, Phys. Rev. B **81**, 081204(R) (2010).
[5]A. V. Kolobov, P. Fons, A. I. Frenkel, A. L. Ankudinov, J. Tominaga, and T. Uruga, Nature Mater. **3**, 703 (2004).
[6]S. Caravati, M. Bernasconi, T. D. Kühne, M. Krack, and M. Parrinello, Appl. Phys. Lett. **91**, 171906 (2007).
[7]J. Akola and R. O. Jones, Phys. Rev. B **76**, 235201 (2007).
[8]Z. Sun, J. Zhou, and R. Ahuja, Phys. Rev. Lett. **98**, 055505 (2007).
[9]J. Hegedüs and S. R. Elliott, Nature Mater. **7**, 399 (2008).
[10]J. Im, E. Cho, D. Kim, H. Horii, J. Ihm, and S. Han, Phys. Rev. B **81**, 245211 (2010).
[11]J. Akola, J. Larrucea, and R. O. Jones, Phys. Rev. B **83**, 094113 (2011).
[12]E. Cho, J. Im, C. Park, W. J. Son, D. H. Kim, H. Horii, J. Ihm, and S. Han, J. Phys.: Condens. Matter **22**, 205504 (2010).
[13]J. Akola and R. O. Jones, J. Phys.: Condens. Matter **20**, 465103 (2008).
[14]A. V. Kolobov, P. Fons, M. Krbal, R. E. Simpson, S. Hosokawa, T. Uruga, H. Tanida, and J. Tominaga, Appl. Phys. Lett. **95**, 241902 (2009).
[15]J. P. Perdew, K. Burke, and M. Ernzerhof, Phys. Rev. Lett. **77**, 3865 (1996).
[16]M. Micoulaut, R. Vuilleumier, and C. Massobrio, Phys. Rev. B **79**, 214205 (2009).
[17]G. Kresse and J. Hafner, Phys. Rev. B **47**, 558 (1993).
[18]P. E. Blöchl, Phys. Rev. B **50**, 17953 (1994).
[19]A. D. Becke, Phys. Rev. A **38**, 3098 (1988).
[20]C. Lee, W. Yang, and R. G. Parr, Phys. Rev. B **37**, 785 (1988).
[21]A. V. Krukau, O. A. Vydrov, A. F. Izmaylov, and G. E. Scuseria, J. Chem. Phys. **125**, 224106 (2006).
[22]J. P. Perdew, M. Ernzerhof, and K. Burke, J. Chem. Phys. **105**, 9982 (1996).
[23]S. Park, B. Lee, S. H. Jeon, and S. Han, Curr. Appl. Phys. **11**, S337 (2011).
[24]M. A. L. Marques, J. Vidal, M. J. T. Oliverira, L. Reining, and S. Botti, Phys. Rev. B **83**, 035119 (2011).
[25]S. Kohara, K. Kato, S. Kimura, and H. Tanaka, Appl. Phys. Lett. **89**, 201910 (2006).
[26]P. Jóvári, I. Kaban, J. Steiner, B. Beuneu, A. Schöps, and A. Webb, J. Phys.: Condens. Matter **19**, 335212 (2007).
[27]V. F. Sears, Neutron News **3**, 29 (1992).
[28]C. Steimer, V. Coulet, W. Welnic, H. Dieker, R. Detemple, C. Bichara, B. Beuneu, J.-P. Gaspard, and M. Wuttig, Adv. Mater. **20**, 4535 (2008).
[29]A. L. Ankudinov, B. Ravel, J. J. Rehr, and S. D. Conradson, Phys. Rev. B **58**, 7565 (1998).
[30]A. V. Poiarkova and J. J. Rehr, Phys. Rev. B **59**, 948 (1999).
[31]M. Kuwahara, O. Suzuki, Y. Yamakawa, N. Taketoshi, T. Yagi, P. Fons, T. Fukaya, J. Tominaga, and T. Baba, Jpn. J. Appl. Phys., Part 1 **46**, 3909 (2007).
[32]A. J. Cohen, P. Mori-Sánchez, and W. Yang, Science **321**, 792 (2008).
[33]E. Cho, Y. Youn, and S. Han, Appl. Phys. Lett. **99**, 183501 (2011).
[34]M. Krbal, A. V. Kolobov, P. Fons, J. Tominaga, S. R. Elliott, J. Hegedus, and T. Uruga, Phys. Rev. B **83**, 054203 (2011).
[35]M. Naito, M. Ishimaru, Y. Hirotsu, R. Kojima, and N. Yamada, J. Appl. Phys. **107**, 103507 (2010).
[36]D. A. Baker, M. A. Paesler, G. Lucovsky, S. C. Agarwal, and P. C. Taylor, Phys. Rev. Lett. **96**, 255501 (2006).
[37]P. Jóvári, I. Kaban, J. Steiner, B. Beuneu, A. Schöps, and M. A. Webb, Phys. Rev. B **77**, 035202 (2008).
[38]A. V. Kolobov, M. Krbal, P. Fons, J. Tominaga, and T. Uruga, Nature Chem. **3**, 311 (2011).
[39]T. H. Jeong, M. R. Kim, H. Seo, J. W. Park, and C. Yeon, Jpn. J. Appl. Phys., Part 1 **39**, 2775 (2000).